



OPEN

Understanding carbon resilience under public health emergencies: a synthetic difference-in-differences approach

Chengke Wu¹, Xiao Li², Rui Jiang¹, Zisheng Liu¹, Fangyun Xie³, Juan Wang², Yue Teng⁴ & Zhile Yang¹✉

Public health emergencies influence urban carbon emissions, yet an in-depth understanding of deviations between regional emissions under such emergencies and normal levels is lacking. Inspired by the concept of resilience, we introduce the concept of regional carbon resilience and propose four resilience indicators covering periods during and after emergencies. A synthetic difference-in-differences model is employed to compute these indicators, providing a more suitable approach than traditional methods assuming unchanged levels before and after emergencies. Using the COVID-19 pandemic in China as a case study, focusing on the power and industry sectors, we find that over 40% regions exhibit strong resilience (> 0.9). Average in-resilience (0.764 and 0.783) is higher than post-resilience (0.534 and 0.598) in both sectors, indicating lower resilience during than after emergencies. Significant differences in resilience performance exist across regions, with Hebei (0.93) and Hangzhou (0.92) as top performers, and Qinghai (0.29) and Guiyang (0.36) as the least resilient. Furthermore, a preliminary correlation analysis identifies 22 factors affecting carbon resilience; higher energy consumption, stronger industrial production, and a healthier regional economy positively contribute to resilience with coefficients over +0.3, while pandemic severity negatively impacts resilience, with coefficients up to -0.58. These findings provide valuable references for policymaking to achieve carbon neutrality goals.

Decarbonization lies in the centre of urban sustainability, with over 198 countries committed to achieving carbon neutrality. Various decarbonization strategies have been implemented, generally grouped into carbon mitigation and adaptation, both requiring efforts in technology development and policymaking¹. Carbon mitigation aims to reduce carbon emissions. One widely recognized strategy is the implementation of hybrid energy systems combining energy storage with two or more renewable energy sources, such as solar, wind, hydropower, bioenergy, and geothermal. Projections suggest that renewable energy will comprise 74% of global energy production by 2050². Typical carbon mitigation policies include carbon pricing, taxing, and trading, targeting sectors that account for most CO₂ emissions, such as power generation, industrial manufacturing, transportation, residential usage, and agriculture^{3,4}. On the other hand, carbon adaptation highlights preparing for and adapting to changes already caused by increased emissions. The strategies focus on developing resilient and sustainable cities and infrastructures, so that the society suffers less from climate shocks or can quickly recover from damages. From a technical perspective, carbon adaptation may involve the development of advanced systems for data monitoring, risk warning, hazard prediction, and emergency response⁵. Representative government initiatives include enacting regulations and standards for measuring infrastructure resilience, ensuring energy security, and providing social protection after disasters^{1,3}.

Implementing decarbonization strategies requires consistent coordination of technologies, policies, and resources of multiple parties. Predictable emission levels and trends are critical for maintaining these efforts⁴. However, current strategies overlook a potential factor that can introduce significant uncertainty into decarbonization plans and predictions: public health emergencies (PHEs)^{6–8}. PHEs impact numerous aspects of modern

¹Shenzhen Institute of Advanced Technology, Chinese Academy of Sciences, Shenzhen, China. ²Faculty of Engineering, The University of Hong Kong, Hongkong SAR, China. ³Chongqing Economic and Social Development Research Institute, Chongqing, China. ⁴Department of Building and Real Estate, the Hong Kong Polytechnic University, Hongkong SAR, China. ✉email: zl.yang@siat.ac.cn

cities, including carbon emissions. The global PHE caused by COVID-19 resulted in nearly 7 million deaths and substantial economic losses⁹. To contain the virus, aggressive measures were implemented, including mandated quarantines and nucleic acid testing, prohibition of social gatherings, transportation restrictions, and city-wide lockdowns^{10,11}. Consequently, carbon emissions in many cities exhibited marked fluctuations. Numerous studies have examined CO₂ emissions during the COVID-19 pandemic and discovered that prevention measures contributed to a global reduction in CO₂ emissions by up to 30%^{10,12–14}. However, these studies focused on the initial outbreak period of 2019, overlooking the extended effects over the entire three years. The initial decrease in CO₂ emissions may rebound after the pandemic, potentially dropping far below or surpassing the previous levels, thereby complicating existing decarbonization plans and policies. For instance, resources and policy attention could be reallocated from regions experiencing significant emission declines due to the pandemic to those encountering emission increases. Consequently, there is a crucial need to precisely evaluate emission variance and divergence to ensure the timely adjustment of decarbonization plans and fulfilment of carbon reduction objectives. However, a robust method for this purpose is notably lacking.

Inspired by the concept of resilience^{15–17}, we proposed regional carbon resilience to evaluate a region's ability to maintain or recover to its current and predicted emission levels during and after shocks like PHEs. Resilience was first proposed by Holling in the field of economy, who highlighted two types of resilience, namely, engineering and ecological resilience¹⁸. Engineering resilience refers to an economy's ability to 'bounce back' from shocks to a pre-shock level, while ecological resilience refers to the ability to absorb shocks and maintain the current level as long as the magnitude of shock does not surpass a threshold^{15,19}. The concept has also been adopted by scholars in urban development and sustainability. Relevant literature defines resilience as the ability of an urban infrastructure system, e.g., roads, to maintain continuity through shocks and stresses while positively adapting and transforming towards sustainability. As shown in Supplementary Fig. 1, current urban resilience considers four dimensions: i.e., robustness, rapidity, redundancy, and resourcefulness¹⁷. Robustness evaluates the differences between actual and expected infrastructure functionality. Rapidity indicates the capacity to restore previous functionality of the infrastructure in a timely manner. Redundancy determines the extent to which infrastructure preserves basic functionalities under significant degradation or damage. Resourcefulness implies the ability to diagnose and handle emergencies by taking adaptive measures, such as identifying and allocating resources^{20–22}. Additionally, many argue that measuring resilience is more meaningful during sudden disturbances rather than slow-burning process²³.

However, existing resilience evaluation methods have two limitations when applied to PHEs. First, CO₂ emissions in a region exhibit trends and fluctuations regardless of PHEs, and resilience should be evaluated based on the difference between these two curves. However, classical methods tend to assume that the normal emissions remain unchanged throughout PHEs. Second, bouncing back or even beyond is favourable in conventional resilience, which is the opposite in the context of CO₂ emissions. Moreover, significant and sustained declines in emissions without recovery should also be warned, because they may lead to a misallocation of decarbonization resources that could be utilized more effectively elsewhere.

To address these limitations, we aimed to develop four counterfactual regional carbon resilience indicators by leveraging a causal effect evaluation model, synthetic difference-in-differences (Syn-Did)^{24,25}. The Syn-Did effectively models the counterfactual trend of CO₂ emissions in the absence of PHEs, rather than simply assuming they remain unchanged before and after PHEs, as traditional methods do. We drew upon urban resilience indicators while modifying the algorithm, which allowed us to classify regions experiencing significant emissions declines or increases beyond previous levels as having low resilience. Detailed information is available in the Methods section. We selected China as the research subject and COVID-19 as the representative case of PHE for several reasons: (1) China is committed to an ambitious dual-carbon goal to peak emissions by 2030 and achieve carbon neutrality by 2060²⁶; (2) during the three-year pandemic, China implemented stringent prevention measures, providing a rich dataset for PHE investigations^{10,27}; (3) COVID-19's widespread and far-reaching influences²⁸ can help form a comprehensive understanding of the impacts of PHEs on CO₂ emissions^{14,29,30}. The evaluation focuses on the power generation and industrial manufacturing sectors, excluding other sectors owing to data quality considerations. These two sectors account for 44% and 38% of total emissions in China, respectively²⁶, which can offer representative results and valuable insights.

Using the proposed method, we identified regions with the lowest (e.g., Qinghai, Guiyang) and highest (e.g., Jiangsu, Hangzhou) carbon resilience from a spatial perspective. Temporally, we observed greater carbon resilience during pandemics than subsequent periods, in other words, CO₂ emissions are more likely to diverge from the pre-pandemic levels once the pandemic ends. We also identified four distinct emission patterns: fluctuating, insensitive-to-impact, diverging-declining, and diverging-surpassing. Additionally, a preliminary correlation analysis identified 22 factors influencing carbon emissions resilience. In summary, the study investigates the impacts of PHEs on regional CO₂ emissions, an uncovered area in decarbonization and urban sustainability. The findings provide novel and useful references for decarbonization policymaking to address shocks caused by PHEs. Furthermore, since emissions represent just one facet of regional sustainability, the findings and methods offer valuable insights for examining other socio-economic dimensions, such as regional economies and social well-being, in response to shocks that may lead to sustained restrictions on social activities.

Methods

Figure 1 outlines our research design.

Data sources

Both PHE responses and CO₂ emissions data were collected. To ensure evaluation representativeness, we screened 262 publicly reported PHEs in the Wikipedia database, all of which experienced stringent control measures with

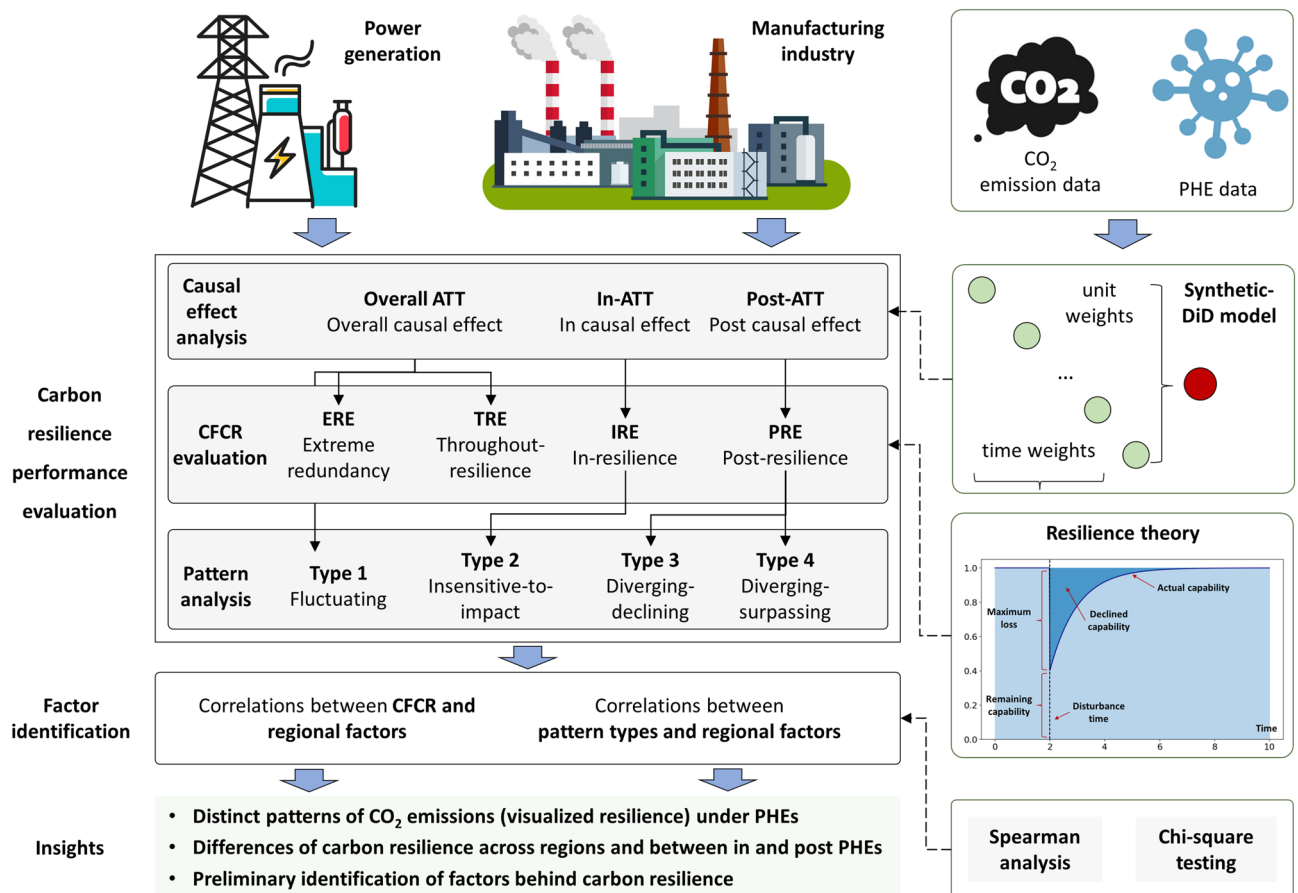


Figure 1. Overall research design, including carbon resilience performance evaluation and preliminary factor identification. The carbon resilience performance evaluation followed three steps. First, absolute causal effects, or average treatment effects on the treated (ATT) on regional carbon emissions were estimated with the Syn-DiD model. We studied both the pandemic period and the period after and computed the ATTs during PHE (in-ATT), ATTs after PHE (post-ATT), and ATTs over the period (throughout-ATT). Second, four carbon resilience indicators were computed based on the ATT results: throughout-resilience, in-resilience, post-resilience, and redundancy. These indicators revealed the regional carbon resilience throughout the period, during PHE, after PHE, and under extreme situations, respectively (see supplementary Table 1). Then, we identified four distinct emission patterns based on the carbon resilience performance: (1) fluctuating, (2) insensitive-to-impact, (3) diverging-declining, (4) diverging-surpassing. Factor identification explored and revealed significant factors influencing the counterfactual carbon resilience and patterns. Accordingly, domain-specific factors, regional socio-economic factors, and PHE-related factors were included in a correlation analysis. Further analysis, such as regression analysis, was not conducted due to the absence of monthly or daily data.

different durations. We named PHEs by the region's name and highlighted them by the italic font. If one region encountered multiple PHEs, we distinguished them by numbers, e.g., *Beijing¹* and *Beijing²*. 67 PHEs with severe consequences in 41 provinces or central cities were selected to further investigate the responses. The initially identified 262 PHEs were reported both at province and city level, which were filtered as follows. All provinces were included, while a city was excluded if not being recognized as a central city, according to the China City Report³¹. As a result, the scope was narrowed down to 105 PHEs. We then filtered out PHEs from ATT analysis and CFR evaluation if the number of confirmed infection cases < 100, which were kept for fitting the Syn-DiD model though. We focused on severe PHEs on the province and central city level, because such PHEs often drew nation-wide attention, which to some extent ensured data richness and reliability, while minimizing uncertainties caused by incrementally intensified prevention measures in local governments. In addition, it could be uncertain for governments to enforce prevention measures until the severity of PHEs reached a threshold³². As such, we established a dataset including 67 PHEs and their corresponding responses in 41 regions of China, covering 19 provinces and four municipalities, i.e., Chongqing, Tianjin, Beijing, and Shanghai.

We collected CO₂ emissions at a day-by-region level, covering 89,790 data points from 2020 to 2022. We incorporated three distinct periods: pre-pandemic (1.5 times the pandemic duration prior to the start of the lockdown), during the pandemic (from the start of the lockdown to its conclusion), and post-pandemic (0.5 times the pandemic duration following the end of the lockdown). As China fully lifted COVID-19 controls in December 2022, and with few cities still experiencing lockdowns at that time, the data from 2020 to 2022 were deemed sufficient for the analysis. All CO₂ emissions data were obtained from the Carbon Monitoring (CM)

project, which was launched and maintained by a joint effort from several top-level universities and institutions. This project has been monitoring daily CO₂ emission data since 2019 based on heterogeneous public sources in different countries. The database included CO₂ emissions emitted by power generation and industry production activities across 13 countries and over 100 regions, including Chinese provinces and municipalities^{33,34}. We directly extracted emissions from the website <https://carbonmonitor.org/>. When it comes to central cities not included in the database, e.g., Xian and Wulumuqi, we estimated their emissions in power generation and industrial production by distributing CO₂ emissions in the corresponding province based on electricity production and secondary industry GDP, respectively. Finally, to collect the values of factors for correlation testing, we searched other sources, such as yearbooks downloaded from government databases and the WIND database <https://www.wind.com.cn/>.

Syn-Did model for causal effect analysis

We adopted Syn-Did to estimate causal effects under PHE responses. The essence is to estimate the counterfactual emissions if a region under a PHE had not encountered such shocks. Simply put, the Syn-Did can be seen as an optimization model that: (1) based on regional features, estimates optimal weights of all regions not affected by the same PHE happening in the studied region, (2) simulates the counterfactual emission by summing the weighted emissions of the unaffected regions. For example, to estimate the counterfactual emissions in Wuhan, the Syn-Did model identified Chongqing and Changsha as regions unaffected by the PHE and having similar characteristics to Wuhan. The model then calculated the optimal weights for these two cities to create a virtual city that closely resembles Wuhan. These weights were used to combine the actual emissions from Chongqing and Changsha, thereby estimating the counterfactual emissions for Wuhan.

As presented in Eq. (1), Syn-Did works on a matrix D . Rows and columns in D represent days and regions, respectively. Syn-Did observes regions across time, i.e., days. On a specific day, some regions are treated, and others are not. $Y(T)$, $T \in (0,1)$ is the dependent variable, i.e., CO₂ emissions. The term T refers to the existence of the treatment. $T = 1$ indicates an event leading to causal effects, which is PHE in the study, otherwise $T = 0$. There are two groups of subscripts. The first group includes *pre* and *post*, indicating if a day t is before or after treatment T ; the second group includes *co* and *tr*, indicating if a region is treated. All regions not treated form the control group C . For instance, $Y(0)_{pre,tr}$ and $Y(1)_{post,tr}$ are the actual emissions of the treated region before and after PHE, respectively; $Y(0)_{post,tr}$ is the counterfactual emissions without PHE in the post-treatment period. The causal effect ATT is estimated following Eq. (2). To predict $Y(0)_{post,tr}$, Syn-Did crafts a virtual region by combining control units, i.e., regions $\in C$, aiming to minimize the difference of $Y(0)_{pre}$ between the virtual and treated regions. The higher the similarity between the two regions, the more reliable the causal effects.

When implementation, given a region of interest, we used rule-based filtering to exclude regions experiencing PHE in both pre- and post-pandemic periods, allowing the remaining regions to form the group C . Then, we applied convex optimization to determine the weights of regions in C and form a vector $\omega_{co} \in R^C$. We generated $Y(0)_{post,tr}$ by integrating emissions of the control units during the pre-treatment period (Eq. (3)). The $\xi T_{pre} \|\bullet\|$ is the regularization term for stabilizing optimization, and details can be found in Ref.^{24,35}. Additionally, specific temporal patterns also affect model fitting. For instance, the Chinese Spring Festival and seasonal demands can cause large emission variances. To minimize the difference between pre- and post-treated periods among control units, we applied a similar optimization process to evaluate another vector $\lambda_{pre} \in R^E$ recording the weight for each day before PHE (Eq. (4)). Finally, we integrated the unit and time weights into the weighted linear square model to produce $Y(0)_{post,tr}$ and ATT s.

$$D = \begin{bmatrix} 0 & 0 & \cdots & 0 & 0 \\ 0 & 0 & \cdots & 0 & 0 \\ \vdots & \vdots & \ddots & \vdots & \vdots \\ 0 & 0 & \cdots & 1 & 1 \\ 0 & 0 & \cdots & 1 & 1 \end{bmatrix} = \begin{bmatrix} Y(0)_{pre,co} & Y(0)_{pre,tr} \\ Y(0)_{post,co} & Y(1)_{pre,tr} \end{bmatrix} \quad (1)$$

$$ATT = Y(1)_{post,tr} - Y(0)_{post,tr} \quad (2)$$

$$\begin{cases} \omega_{co} = \underset{\omega}{\operatorname{argmin}} \|\bar{y}_{pre,tr} - (Y_{pre,co} * \omega_{co} + \omega_0)\|_2^2 + \xi T_{pre} \|\omega_{co}\|_2^2 \\ s.t \sum \omega_i = 1 \text{ and } \omega_i > 0 \forall i \in C \end{cases} \quad (3)$$

$$\begin{cases} \lambda_{pre} = \underset{\lambda}{\operatorname{argmin}} \|\bar{y}_{post,co} - (\lambda_{pre} * Y_{pre,co} + \lambda_0)\|_2^2 \\ s.t \sum \lambda_t = 1 \text{ and } \lambda_t > 0 \forall t \end{cases} \quad (4)$$

Counterfactual carbon resilience evaluation

We drew upon the concept of resilience and proposed four counterfactual carbon resilience indicators based on ATT values. Supplementary Fig. 1b illustrates the key concept. We defined carbon resilience as the reciprocal of the areas caused by emission curves diverging from the counterfactual baseline. Equation (5) presents the calculation, where A , N_i and N_j are the area, starting time, and ending time, respectively. Since both declining below and surging above the baseline are unfavourable, we expected the total area between actual and simulated

emissions to be as small as possible, thereby resulting in larger reciprocal values and higher resilience. The baseline was defined as the minimum value of the two curves during the studied period, which could make the disturbance more distinctive.

$$resilience = 1 / \int_{N_i}^{N_j} A \quad (5)$$

To enable comprehensive evaluation, we divided the entire period into three sub-periods. As such, the throughout resilience, in-resilience, and post-resilience could be evaluated by Eq. (5), with different settings of N_i and N_j . We supposed that the PHE happened at N_0 ; the first sub-period started N_1 months prior to N_0 ; the second sub-period covered the pandemic lasting N_2 months; the third sub-period started when the PHE ended, while extending N_3 months thereafter. N_0 and N_2 could be directly obtained by referring to public PHE data, based on which N_1 and N_3 were dynamically evaluated. Specifically, we defined $N_1 = 1.5N_2$ and $N_3 = 0.5N_2$, thereby ensuring $N_2 \geq N_1 + N_3$. The setting provided adequate data for fitting Syn-DiD before PHEs while minimizing evaluation errors after PHEs. As such, the throughout resilience, in-resilience, and post-resilience were evaluated following adjusted equations in Table 1.

We also evaluated redundancy which is defined in Table 1. In this case, smaller differences under extreme situations indicated low vulnerability and strong resilience. The fourth row in Table 1 presents the equation, where $Y(0)_{post,tr}$ and $Y(1)_{post,tr}$ are the simulated and actual emissions in the studied region, respectively. Finally, one region could be evaluated multiple times if it encountered more than one PHEs. In that case, we averaged the results as the final counterfactual carbon resilience indicators for the region.

Emission pattern analysis

We categorized emission patterns under PHE by combining qualitative interpretation and quantitative ATTs results. Specifically, if the actual and counterfactual emission curves crossed each other for at least one time since the PHE began, we categorized the emission pattern as the fluctuating type (Type-1); if the in-resilience of the region under one PHE was larger than 0.9, we defined the pattern as insensitivity-to-impact (Type-2); if the post-resilience of the region under one PHE was less than 0.9, we defined the pattern as diverging, which fell into the diverging-declining (Type-3) type and diverging-surpassing type (Type-4) if the emission was below and above the counterfactual baseline, respectively.

Preliminary factor identification through correlation testing

We identified 64 factors through literature review. The full factor lists are in Supplementary Tables 2–4. The power and industry sectors each involved 21 factors, and there were 19 and three factors reflecting social-economic development level and PHE severity, respectively. Then, we invited 16 domain experts and conducted a survey. We organized online or in-person meetings with each expert, briefed them on the research purpose and methods and definitions of factors in case there was ambiguity and confusion. Then, we asked them to identify significant factors affecting regional emissions under PHEs using a 5-level rating scale. More information of the expert surveying can be found in the supplementary survey information. We kept factors obtaining an average score > 3.0 in the correlation testing. The survey resulted in 27 and 22 factors for power generation and industrial production, respectively (Supplementary Tables 2–4). We denoted $R(s)$ as the set of factors in a sector $s \in (power, industry)$. We used Spearman analysis and Chi-square testing to reveal factors significantly affecting pattern categories and counterfactual carbon resilience results, respectively.

Spearman analysis is a popular dependence measure between two continuous variables. The method supposes a monotonic relationship between two variables, while having few other assumptions and restrictions in terms of data distributions. It also works well in small sample sets, making it suitable in our case³⁶. We evaluated the Spearman coefficient ρ using Eq. (6), where x_i and y_s refer to affecting factors and counterfactual carbon resilience indicators, respectively, and $i \in R(s)$. We set the confidence level at 0.05 for Spearman analysis, considering the data requirements and initial testing results³⁶.

$$\rho = \sum_{i,s} (x_i - \bar{x})(y_s - \bar{y}) / \sqrt{\sum_{i,s} (x_i - \bar{x})^2 (y_s - \bar{y})^2} \quad (6)$$

Chi-square testing is a useful method when investigating correlations of discrete variables. The results are represented in matrices, where the horizontal and vertical axis refers to independent factors and dependent variables, i.e., emission pattern types, respectively. Each cell in a matrix indicates the membership of the regions. To

Indicator	Definition	Starting time (N_i)	Ending time (N_j)	Equation
In-resilience	Resilience from the onset of PHEs until their conclusion	$N_0 - N_1$	$N_0 + N_2$	$1 / \int_{N_0 - N_1}^{N_0 + N_2} A$
Post-resilience	Resilience after PHEs ended	$N_0 + N_2$	$N_2 + N_3$	$1 / \int_{N_0 + N_2}^{N_2 + N_3} A$
Throughout-resilience	Resilience covering the entire studied period	$N_0 - N_1$	$N_2 + N_3$	$1 / \int_{N_0 - N_1}^{N_2 + N_3} A$
Redundancy	The reciprocal of the absolute maximum discrepancy between the actual and counterfactual emissions in the entire studied period	$N_0 - N_1$	$N_2 + N_3$	$1 / \max Y(0)_{post,tr} - Y(1)_{post,tr} $

Table 1. Resilience indicator evaluation equations.

enable Chi-square testing, we converted counterfactual carbon resilience indicators and continuous independent factors into discrete ones with quantile segmentation. To comply with the requirement that the theoretical number of samples in each cell in the Chi-square matrix should be larger than five³⁷, we combined the first and last two quantiles of factor values, which resulted in matrices $\in \mathbb{R}^{2 \times 4}$. The default hypothesis H_0 is that a region has identical probability to fall in any cell when a factor is not relevant to the categories, and we should observe five regions in each cell. As such, the Chi-square statistic χ^2 is estimated with Eq. (7). If χ^2 is larger than zero by a threshold, H_0 is rejected and the factor is recognized as significant. The threshold follows the Chi-square distribution and depends on the confidence level and degree-of-freedom (DoF). In our case, the DoF is three, and we set the confidence level as 0.1, leading to a Chi-square threshold of 6.25³⁷.

$$\chi^2 = \sum_{i=1}^{R(s)} (n_i - np_i)^2 / np_i \quad (7)$$

Results

Overview of emissions variances under PHE

Figure 2 shows percentage differences in CO₂ emissions for each year from 2020 to 2022, compared to that in 2019. According to the figure, the large emission decline mentioned in previous studies was reflected in the first half of 2019, where the power and industry emissions were reduced by up to 40% and 30%, respectively. However, for the majority of the remaining periods, the emission curves exceeded the 2019 baseline and presented a convergence trend regardless of enhanced transmissibility of virus³⁸. This finding complied with some studies suggesting minor emission differences caused by COVID-19³⁹. The emission increase could be attributed to the continuous introduction of economic stimulus policies and improvements of control measures, and we regarded the convergence as a manifestation of the sectors' adaptation under PHEs. In a word, PHEs, even as severe as COVID-19, were unlikely to alter overall emission trends at the nation level. However, the impacts on specific sectors and regions could be hidden behind the oversimplified nation-level investigation⁴⁰. For instance, emissions declined in one region could be offset by emission increased in another, or emission variances during and after PHEs could counterbalance each other. Thus, uncovering more universal and sophisticated principles of CO₂ emissions under PHEs is important.

Carbon resilience performance evaluation of power sector

Absolute causal effects, or ATTs on carbon emissions estimate the differences between emissions under a pandemic and the counterfactual situations without a pandemic. Here we define a PHE as one lockdown of a region and it should be noted that a few regions have experienced several lockdowns. The overall ATT results showed that 19 PHEs resulted in large CO₂ emission fluctuations over 10,000 t d⁻¹. The PHE, *Gansu*¹ caused the most significant emission increase (26,390 t d⁻¹), followed by *Zhenjiang* (20,730 t d⁻¹), *Henan* (20,700 t d⁻¹), and *Shandong* (20,550 t d⁻¹). Meanwhile, four PHEs resulted in considerable negative ATTs, i.e., *Xinjiang* (−29,360 t d⁻¹), *Hunan*¹ (−25,090 t d⁻¹), *Shanghai* (−23,190 t d⁻¹), and *Zhejiang*¹ (−22,760 t d⁻¹). In contrast, four regions experienced lockdowns with negligible emission disturbances (< 200 t d⁻¹), including *Tianjin* (−20 t d⁻¹), *Qingdao* (−70 t d⁻¹), *Xian* (−130 t d⁻¹), and *Wuhan*¹ (−190 t d⁻¹). Then, we estimated in-ATTs and observed severe emission declines due to PHEs. The effects of *Xinjiang* (−45,360 t d⁻¹) and *Shanghai* (−33,420 t d⁻¹) were salient and substantially exceeded the positive ATTs, e.g., *Shandong* (21,380 t d⁻¹) and *Gansu*¹ (20,520 t d⁻¹). Several PHEs failed to alter CO₂ emissions during pandemics, e.g., *Xining* (10 t d⁻¹), *Tianjin* (−20 t d⁻¹), *Chongqing*¹ (20 t d⁻¹), and *Jilin*¹ (70 t d⁻¹). According to post-ATTs, ending of PHEs was strongly correlated to severer emission disturbances. 15 PHEs caused emission variance > 20,000 t d⁻¹, such as *Zhejiang* (−60,630 t d⁻¹), *Hunan*¹ (−48,940 t d⁻¹), *Anhui* (39,920 t d⁻¹), and *Gansu*¹ (38,860 t d⁻¹). The number of severe PHEs was three times of that in in-ATTs. Meanwhile, there were still only six lockdowns failing to change emissions by > 200 t d⁻¹, and *Tianjin* (−10 t d⁻¹) and *Hainan* (20 t d⁻¹) ranked the first two places.

Counterfactual carbon resilience indicators, calculated based on ATTs, represent regional carbon resilience. A higher indicator value signifies enhanced resilience, with the results displayed in Fig. 3a–d and Supplementary

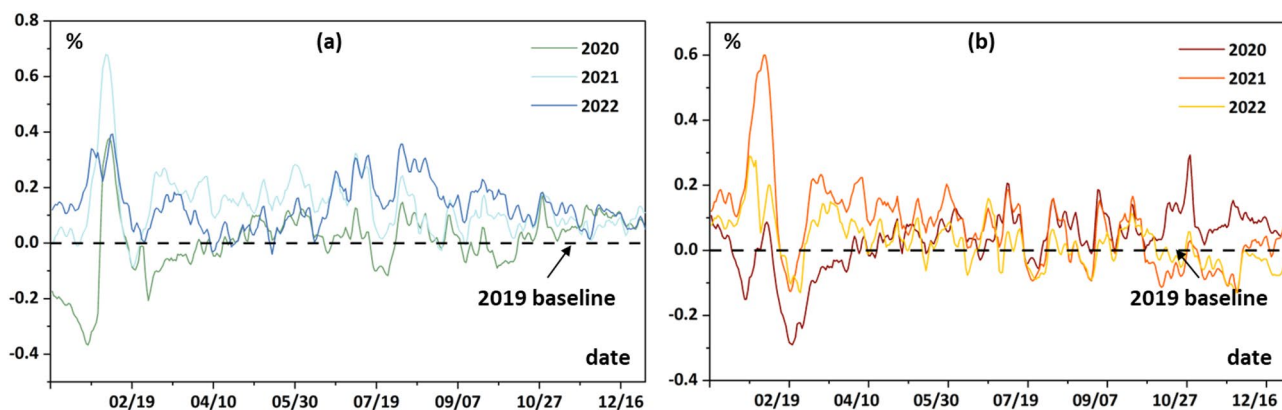


Figure 2. Daily CO₂ emission differences (%) between 2020 and 2022, (a) Power sector, (b) Industry sector.

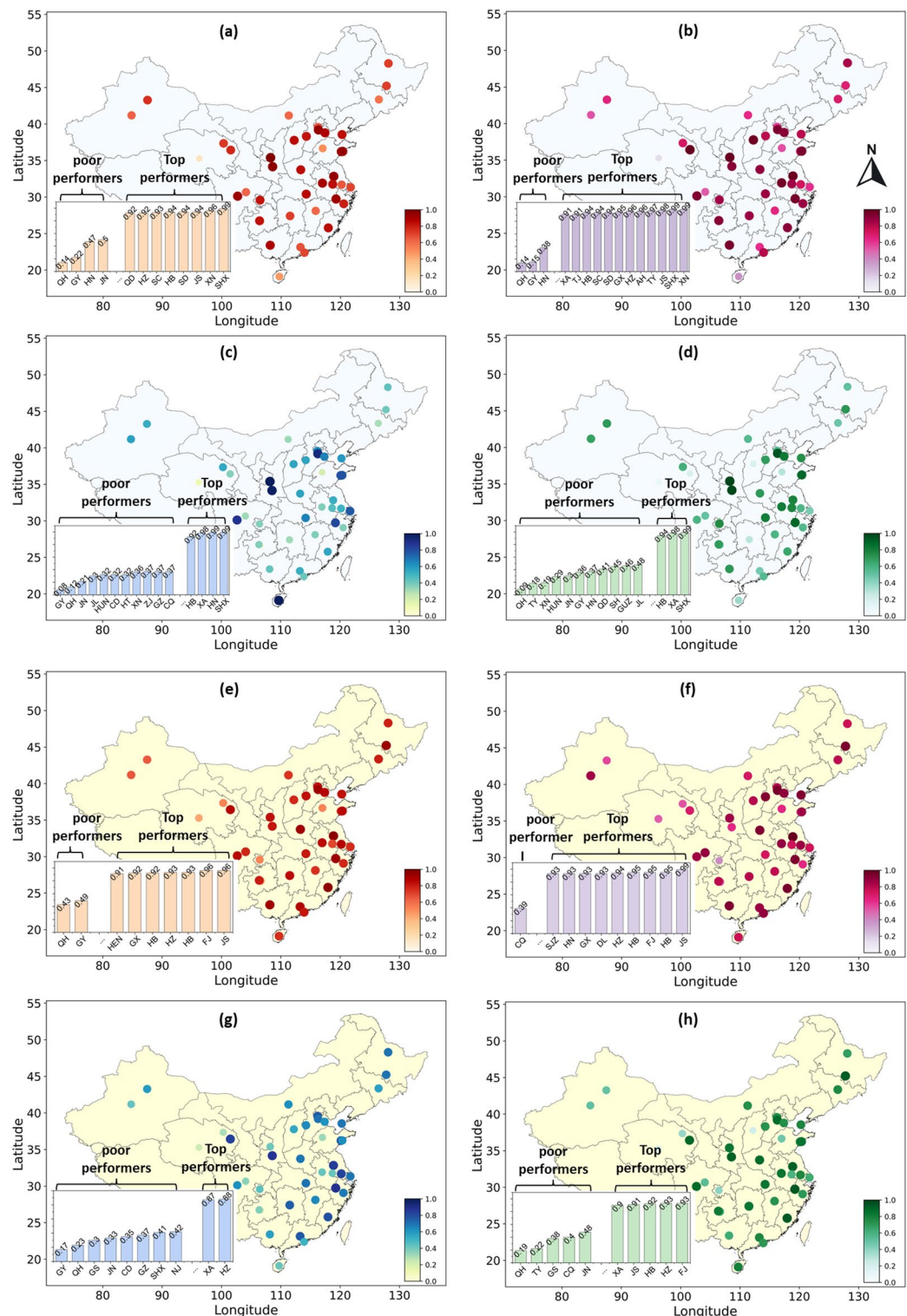


Figure 3. Counterfactual carbon resilience evaluation (region abbreviations are listed in Supplementary Table 1). (a) Throughout-resilience in the power sector, (b) In-resilience in the power sector, (c) Post-resilience in the power sector, (d) Redundancy in the power sector, (e) Throughout-resilience in the industry sector, (f) In-resilience in the industry sector, (g) Post-resilience in the industry sector, (h) Redundancy in the industry sector.

Table 5. Eight regions reached high throughout-resilience > 0.9 . Power emissions in Shaanxi (0.99) and Xian (0.96) were almost immune to lockdowns, and Hebei, Shandong, and Jiangsu (0.94) were the immediate followers. However, Qinghai (0.14), Guiyang (0.22), and Hainan (0.47) were the bottom performers with throughout-resilience < 0.5 . The best and worst members of in-resilience were similar to the throughout group. As for post-resilience, 18 out of 41 regions could not gain post-resilience > 0.5 . The indicators in Guiyang (0.08) and Qinghai (0.12) were quite low. In contrast, higher scores (> 0.8) in post-resilience were only observed in Xian (0.98), Hainan (0.97), Hebei (0.89), and Sichuan (0.88). Finally, several regions outperformed others in terms of redundancy, such as Shaanxi (0.99), Xian (0.98), and Hebei (0.94). Qinghai again revealed its extreme vulnerability, whose redundancy was only 0.09, followed by Taiyuan (0.18) and Xining (0.19).

Based on the calculated ATTs and carbon resilience indicators, four emission patterns were identified. Typical emission curves of regions influenced by the pandemic lockdown are illustrated in Fig. 4a–d. Surprisingly, 40% of PHEs (29/67) followed the insensitive-to-impact pattern (Type-2), and the fluctuating (Type-1), diverging-declining (Type-3), and diverging-surpassing (Type-4) patterns involved 15, 12, and 11 PHEs, respectively. Some emission curves following the Type-2 pattern resulted in subtle emission variances in the entire period, e.g., *Tianjin*, *Qingdao*, *Xian*, *Wuhan*¹, and *Beijing*. However, the stability was not universal after PHEs. Five emission curves of Type-2 still triggered post-ATTs $> 20,000 \text{ t d}^{-1}$, i.e., *Anhui*, *Guizhou*, *Hunan*, and *Jiangsu*, and another two encountered substantial emission decline, i.e., *Zhejiang*¹ and *Jilin*¹. In most Type-1 patterns, the emission curves alternated in leading each other, yet resulted in apparent gaps in the end. However, in some PHEs, the emissions converged, such as *Shanghai*, *Beijing*¹, *Hainan*, and *Xinjiang*, indicating effective restoration to the normal emission level. The diverging-surpassing and diverging-declining patterns were clearly reflected in *Beijing*² and *Guiyang* and *Jilin*, *Guangzhou*¹, and *Dalian*, respectively, where CO_2 emissions exceeded or dropped below the counterfactual baseline by a substantial degree once PHEs started.

Correlation analysis of power sector

Through a correlation analysis between counterfactual carbon resilience and regions, we identified 13 significant factors of counterfactual carbon resilience indicators out of 27 potential influencing factors. Six, four, two, and one affected in-resilience, throughout-resilience, post-resilience, and redundancy, respectively. Figure 5a and Supplementary Tables 8, 9 reveal detailed correlation coefficients. The season factor affected all indicators with coefficients ranging from -0.38 to -0.58 . The season is a proxy of important variables, such as temperature. Since COVID-19 was sensitive to high temperature and ultraviolet rays, colder seasons could worsen PHEs and emission disturbances⁴³. The number of infections also indicated severe pandemic and was another factor reaching -0.38 to -0.43 correlation with throughout and in-resilience. Additional consumption of certain energy sources implied stronger counterfactual carbon resilience. For instance, regions with higher consumption of coal ($+0.34$), industrial electricity ($+0.31$), residential electricity ($+0.30$), and total energy ($+0.33$) were prone to forming greater in-resilience; more petroleum and gas consumption increased throughout and in-resilience with coefficients of $+0.34$ and $+0.32$, respectively. It was also easier for regions with larger secondary GDP ($+0.30$) to stabilize power generation emissions during PHEs. We attributed the contribution of industrial vitality to the relatively autonomous operation of many factories. They could maintain regular production and even ramped up output to meet emergency demands from urban areas, thereby consuming more energy and compensating CO_2 reduction caused by restriction of business and commercial activities in public spaces.

Correlation analysis between pattern types and region of power sector recognized three significant factors that have influences on emission pattern types, see Fig. 5b. The number of infected cases and season again played critical roles. When more people were infected, members of the insensitive-to-impact (Type-2) category were transferred to others with more disturbances. Similarly, if PHEs occurred in colder seasons, the probability of being recognized as insensitive was sharply reduced to 1/5, even though the membership of other types remained invariant. Coal consumption was another significant factor. The emission patterns were clustered in fluctuating (Type-1) across regions with lower coal consumption. However, regions with higher coal consumption were prone to following the Type-2 pattern, with the remaining evenly distributed among the other three types. Namely, the power sector with heavier reliance on coal possessed stronger resilience against PHEs, and the credit partially lied in the well-developed coal-fired electricity infrastructure in China^{26,44}.

Carbon resilience performance evaluation of industry sector

Suggested by the absolute causal effect analysis, 11 regions suffered overall ATTs $> 10,000 \text{ t d}^{-1}$ under 13 PHEs. Those causing large emission increasing included *Tianjin*¹ ($24,500 \text{ t d}^{-1}$) and *Shandong* ($27,640 \text{ t d}^{-1}$), and PHEs resulting in drastic emission drop included *Zhejiang* ($-28,320 \text{ t d}^{-1}$), *Gansu*¹ ($-22,450 \text{ t d}^{-1}$), and *Chongqing* ($-18,470 \text{ t d}^{-1}$). However, five PHEs in different regions exhibited minor overall ATTs $< 200 \text{ t d}^{-1}$, e.g., *Beijing* (10 t d^{-1}), *Haerbin* (-20 t d^{-1}), and *Guangzhou* (80 t d^{-1}). When it comes to in-ATTs, *Zhejiang*¹ ($-25,970 \text{ t d}^{-1}$), *Chongqing* ($-25,610 \text{ t d}^{-1}$), and *Shanghai* ($-20,490 \text{ t d}^{-1}$) emitted much less CO_2 compared to counterfactual baselines; *Tianjin*¹ ($19,850 \text{ t d}^{-1}$) and *Chongqing*¹ ($15,970 \text{ t d}^{-1}$) demonstrated the opposite. On the contrary, *Beijing* (10 t d^{-1}), featured the most stable emissions, while *Haerbin*¹ (-20 t d^{-1}), and *Shijiazhuang* and *Hainan* (-90 t d^{-1}) were not far behind. As for post-ATTs, 20 PHEs altered emissions by $> 10,000 \text{ t d}^{-1}$. *Shandong* stood out by increasing $51,280 \text{ t d}^{-1}$ emission, followed by *Tianjin*¹ ($34,360 \text{ t d}^{-1}$) and *Hebei* ($33,700 \text{ t d}^{-1}$). *Beijing* and *Haerbin*¹ represented the less responsive group, where emissions were only slightly increased by 10 t d^{-1} and reduced by 20 t d^{-1} , respectively.

Figure 3e–h and Supplementary Table 10 shows counterfactual carbon resilience evaluation results across regions. As for throughout-resilience, seven regions were regarded as excessive resilient (> 0.9), where Jiangsu and Fujian (0.96) ranked the first. In contrast, Qinghai (0.43) and Guiyang (0.49) were exposed to considerable overall emission disturbances. Nine regions reached in-resilience > 0.9 , and Jiangsu (0.99) and Hebei, Haerbin,

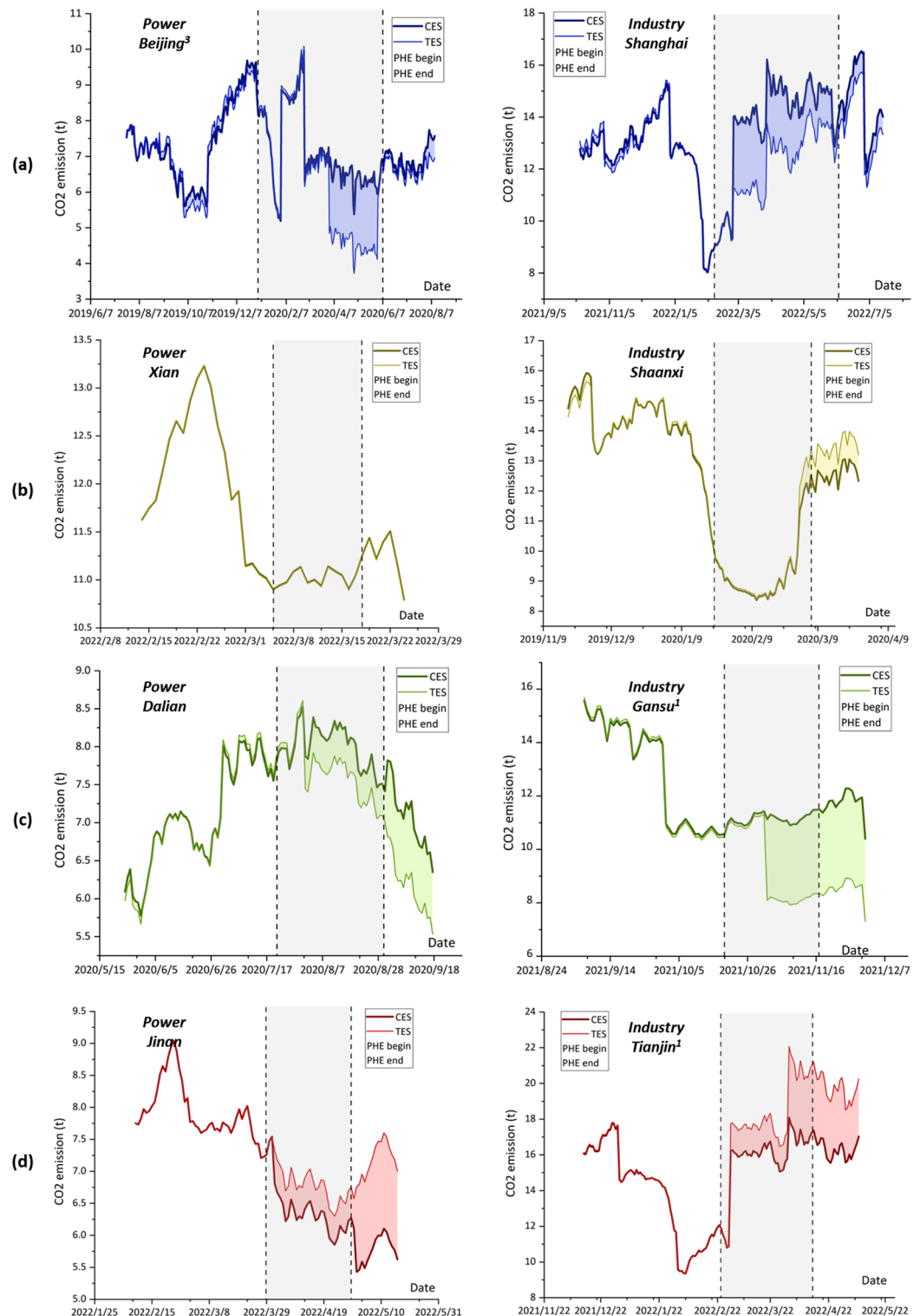


Figure 4. Typical emission patterns under PHEs in the power and industry sector. (a) Pattern type 1, emissions drastically increased or declined when PHEs began and oscillated along the counterfactual baseline. (b) Pattern type 2, there were minor differences between factual and counterfactual emissions, indicating the insensitivity of regional emissions under PHEs, especially during the pandemic. (c) Pattern type 3, emissions dropped in the beginning and struggled to recover, which failed and stayed at a low level when PHEs ended. (d) Pattern type 4, emissions surpassed the counterfactual level by a considerable amount. The latter two patterns could warn potential long-last impact, such as diminished confidence in economy and industry transition^{41,42}. More details can be found in Supplementary Figs. 2–9 and Supplementary Tables 6, 7.

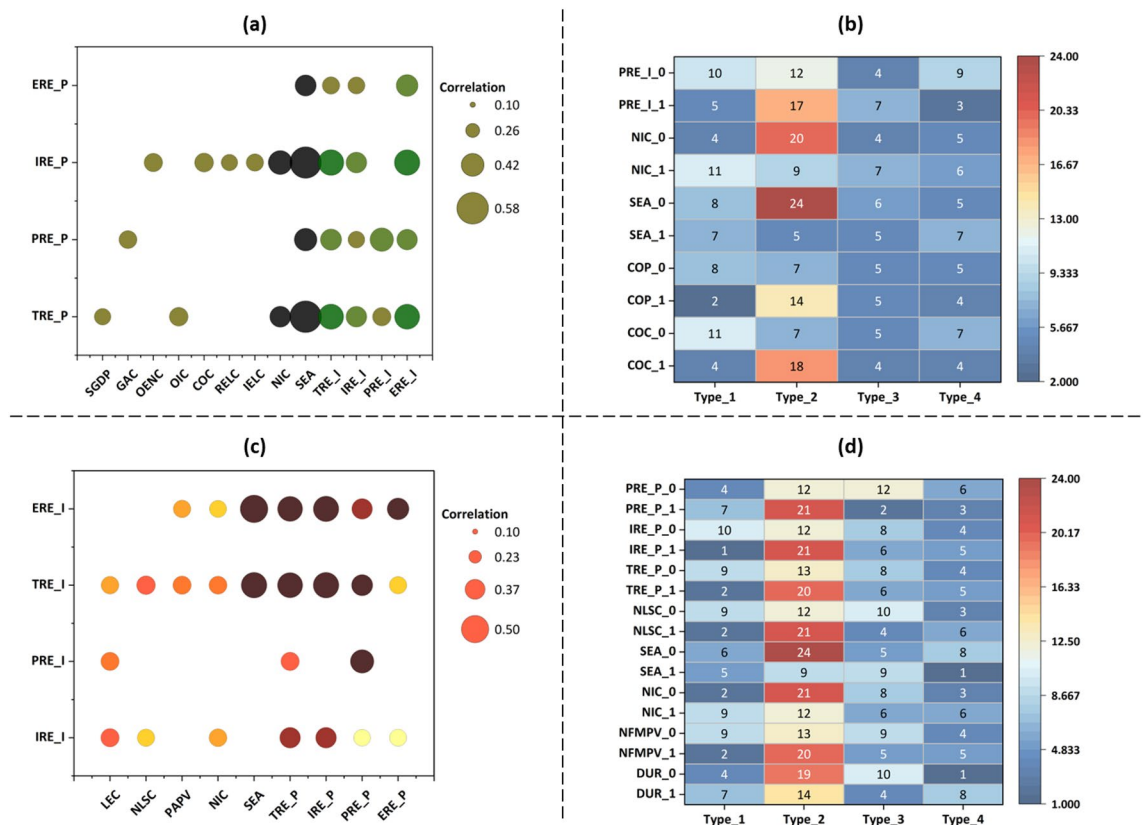


Figure 5. Correlations investigation results. (a) Correlations between resilience indicators and factors in the power sector, (b) Correlations between emission pattern types and factors in the power sector, (c) Correlations between resilience indicators and factors in the industry sector, (d) Correlations between emission pattern types and factors in the industry sector. *ERE* redundancy, *IRE* in-resilience, *PRE* post-resilience, *TRE* throughout resilience; *SGDP* secondary GDP, *GAC* gas consumption, *OENIC* overall energy consumption, *OIC* petroleum consumption, *RELC* residential electricity consumption, *COC* coal consumption, *IELC* industrial electricity consumption, *NIC* the number of infected cases, *SEA* season, *COP* coal production, *LEC* location economy category, *NLSC* the number of large-scale companies, *PAPV* output value of paper production, *NFMPV* output value of the nonferrous metal industry, *DUR* duration; the suffixes 'P' and 'I' indicate the power and industry sector, respectively.

and Fujian (0.95) were the best performers. One city, Chongqing, ended up with a poor in-resilience (0.39), which was the only one failing to reach 0.5. However, when PHEs ended, no regions achieved post-resilience > 0.9. Hangzhou (0.88) and Xian (0.87) performed the best, and other competitors included Jiangsu (0.85), Xining (0.84), and Suzhou (0.83). On the contrary, 12 regions fell into the lowest level (< 0.5) of post-resilience, and Guiyang (0.17) and Qinghai (0.23) suffered excessive poor performance. Industry activities were also sensitive to extreme situations. Only four regions reached the redundancy indicator > 0.9, i.e., Fujian and Hangzhou (0.93), Haerbin (0.92), and Jiangsu (0.91); Qinghai (0.19) and Taiyuan (0.22) were vulnerable in this dimension.

Four emission patterns were also identified for the industry sector, of which the insensitive-to-impact (Type-2) emission pattern was the dominant one, as reflected in 25 out of 67 emission curves. Eight fell into the diverging-surpassing category, and the remaining were distributed into the fluctuating (15) and diverging-declining (12) types. Specifically, *Chongqing*, *Jilin*, and *Shanghai* were representative PHEs, where their emission curves belonged to the Type-1 pattern while presenting the favoured trend of convergence. Among members of Type-2, similar to the power sector, some emissions were insensitive to pandemics in the entire period, such as those under *Beijing*, *Fujian*, *Tianjin*, and *Guangzhou*. However, other members of Type-2 also demonstrated such delayed effects when the PHEs ended, causing the emissions to increase or decline. As for the other two pattern types, *Qinghai*, *Gansu*¹, and *Guiyang* were distinct examples of diverging-declining, and *Jinan* and *Tianjin*¹ clearly presented features of the diverging-surpassing pattern.

Correlation analysis of industry sector

We identified nine significant factors out of 22 candidates through correlation analysis between counterfactual carbon resilience and regions (see Fig. 5c and Supplementary Tables 11, 12). Five, three, three, and one factors were identified to be closely related to throughout-resilience, redundancy, in-resilience, and post-resilience, respectively. Similar to the results of the power sector, season and the number of infection cases interfered with counterfactual carbon resilience indicators. The closer to the winter months, the lower throughout resilience (− 0.46) and redundancy (− 0.50). Meanwhile, 1% increase in infected people reduced the throughout-resilience,

in-resilience, and redundancy by -0.32% , -0.32% , and -0.31% respectively. For industry specific factors, the output value of paper production contributed to throughout-resilience and redundancy with a correlation of $+0.32$. Our guess is that paper production was maintained to produce adequate nucleic acid testing strips. The number of large industrial companies was correlated with throughout-resilience ($+0.34$) and in-resilience ($+0.31$) possibly because many large industrial parks were isolated to sustain normal manufacturing activities. Among social-economic factors, the higher development level of a region, the better it performed in terms of throughout ($+0.32$), in-resilience ($+0.33$), and post-resilience ($+0.33$). Since the latter half of 2020, there were ongoing improvements in epidemic prevention plans^{45,46}. Thus, in more developed regions, the control measures were enforced with greater caution and specificity, and livelihood protection measures were more comprehensive, thereby minimizing PHE impacts.

As shown in Fig. 5d, we found five factors with significant effects on emission categories under PHEs through the correlation analysis between pattern types and regions. These include duration, the number of infected cases and large companies, season, and the output value of non-ferrous metal production. The extended duration of PHEs, coupled with a wider infected population, resulted in reduced membership in the insensitive-to-impact and diverging-declining categories, meanwhile increasing the membership in the fluctuating and diverging-surpassing categories. In addition, regions with larger number of large-scale companies and non-ferrous metal output value tended to sustain baseline emissions, which was reflected by the prevalence of the insensitive-to-impact type. Finally, regions encountered PHEs in colder seasons were less inclined to maintain emissions or surpass the baselines, whereas the likelihood of the diverging-declining pattern was doubled.

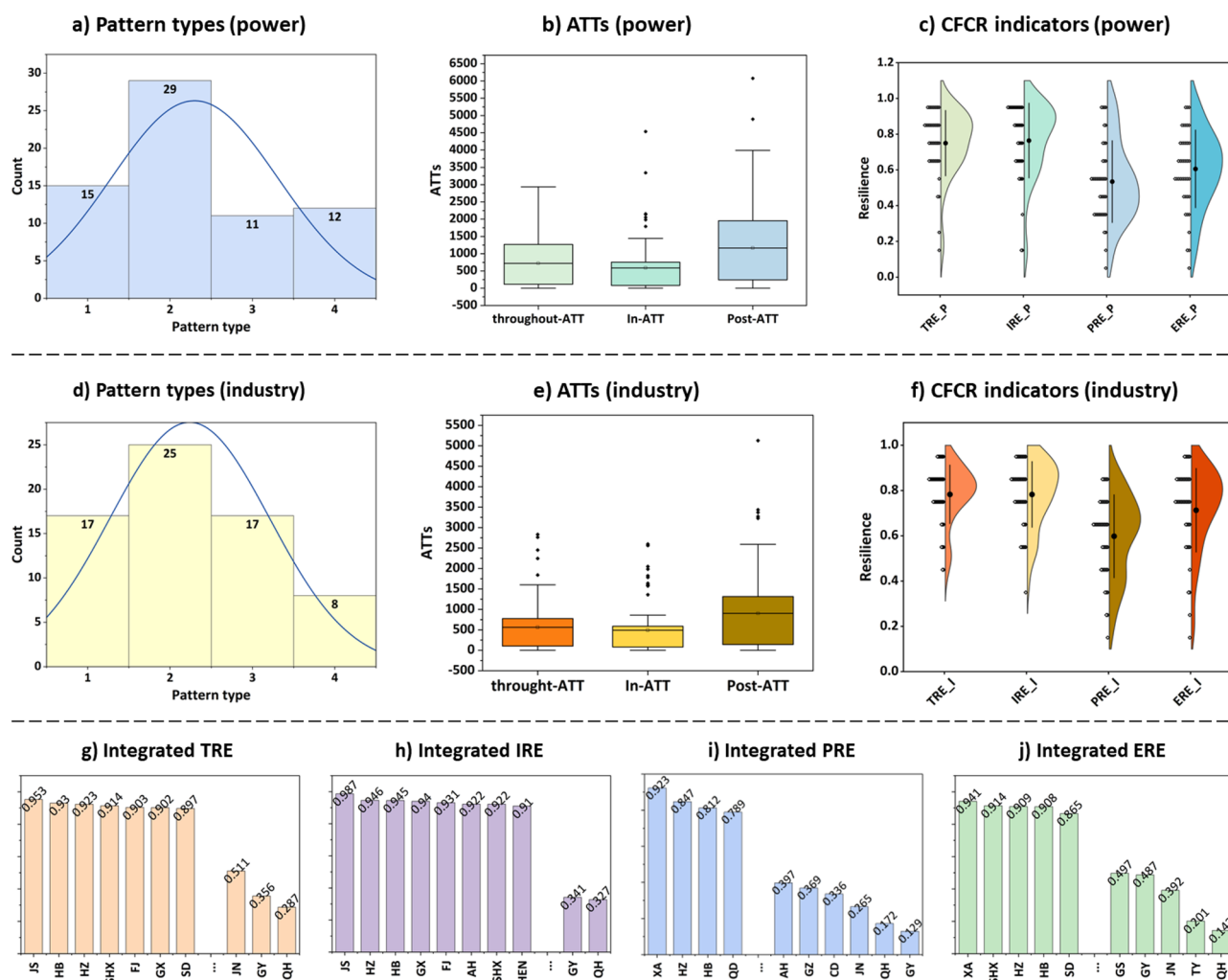


Figure 6. Results of cross-sector investigation. (a) Emission pattern distributions in the power sector, (b) Mean and standard deviations of absolute ATTs in the power sector, (c) Mean and standard deviations of resilience indicators in the power sector, (d) Emission pattern distributions in the industry sector, (e) Mean and standard deviations of resilience indicators in the industry sector, (g–j) Excessively strong and poor resilience in terms of throughout resilience, in-resilience, post-resilience, and redundancy, respectively.

Cross-sector investigation

Based on a cross-sector investigation (see Fig. 6a–j). As presented in Fig. 6b,c, in the power sector, the mean and standard deviations of throughout-ATTs, in-ATTs, and post-ATTs are 722.63 t d^{-1} (789.74 t d^{-1}), 588.58 t d^{-1} (824.66 t d^{-1}), 1162.82 t d^{-1} (1348.65 t d^{-1}), respectively; the same statistics of throughout-resilience, in-resilience, post-resilience, and redundancy in the power sector are 0.750 (0.184), 0.764 (0.210), 0.534 (0.229), 0.606 (0.218), respectively. According to Fig. 6e,f, the mean and standard deviations of absolute throughout-ATTs, in-ATTs, and post-ATTs in the industry sector are 562.58 t d^{-1} (672.27 t d^{-1}), 489.45 t d^{-1} (646.86 t d^{-1}), 901.73 t d^{-1} (1035.63 t d^{-1}), respectively; the statistics of throughout-resilience, in-resilience, post-resilience, and redundancy are 0.783 (0.129), 0.783 (0.145), 0.598 (0.183), and 0.713 (0.185), respectively. As such, we drew several findings from the following aspects.

Sector vulnerability

The industry sector exhibited stronger resilience than the power sector, especially in the post-pandemic period. For the four resilience dimensions, the indicators were 0.33, 0.19, 0.64, and 1.07 higher than those in the power sector, respectively. Meanwhile, the standard deviations of indicators were 0.55, 0.66, 0.46, and 0.33 smaller than those in the power sector, demonstrating superior robustness. This was also reflected by the fact that the throughout-ATTs, in-ATTs, and post-ATTs in the industry sector were 160.05 t d^{-1} , 99.13 t d^{-1} , and 261.09 t d^{-1} less than those in the power sector.

Regional performances

We integrated the counterfactual carbon resilience performance in the two sectors by averaging the four types of indicators and identified two excessive performances, i.e., Hebei and Hangzhou, because they outperformed on all the integrated indicators. Besides, Jiangsu and Fujian performed well for throughout and in-resilience, and Xian excelled in post-resilience and redundancy. On the other hand, Qinghai, Jinan, and Guiyang constantly appeared the most vulnerable regions for most counterfactual carbon resilience indicators in both separated and integrated investigations.

Distributions of emission patterns

The two sectors had similar membership of CO_2 emissions of Type-1 and Type-2. However, it is easier for industrial emissions to decline below the counterfactual baseline. In contrast, power generation emissions were more likely to follow the diverging-surpassing pattern.

Cross-sector counterfactual carbon resilience correlations: As presented in Fig. 5a,c, the throughout-resilience, in-resilience, and redundancy in one sector significantly aligned with most counterfactual carbon resilience indicators in the other with correlation coefficients from +0.30 to +0.47. One exception was the post-resilience in the industry sector, which was only significantly correlated with post- and throughout-resilience in the power sector. This finding complied with our expectation, as the two sectors are closely related²⁶, but emissions were more uncertain in the post-pandemic periods.

Discussion

CO_2 emissions are central to the carbon neutrality strategy and a proxy for vitality in sustainable modern cities. To enhance the predictability of emissions and achieve decarbonization under unexpected events, we introduced the concept of regional carbon resilience and proposed four indicators to interpret resilience and emission patterns. The three-year COVID-19 pandemic in China was revisited as a demonstration case, focusing on the power and industry sectors. Compared with existing studies on decarbonization strategies and resilience, our study features two novel contributions.

First, the study addresses an unexplored area of decarbonization strategies. Current studies focus on long-term strategies, including developing renewable energy technologies and policymaking related to carbon pricing, taxing, trading policies, energy security, and resilient infrastructures^{1–3}. Decarbonization requires close collaboration between governments, with predictable emissions being essential for implementing strategies as planned. However, the consideration of shocks that can cause drastic emission fluctuations is lacking. PHEs, such as COVID-19, serve as a typical example of such shocks, interfering with socio-economic activities and introducing severe uncertainty in regional emissions. Our study contributes by providing a novel perspective for investigating such uncertainty.

Second, to evaluate the emission uncertainty, this study proposes a new method combining causal analysis and resilience measuring. Previous studies of carbon emissions during COVID-19 directly compared emission levels with those of the previous year (i.e., 2019). These results lack interpretability and credibility because they did not capture the temporal trends and changes of emissions. More importantly, they focused on the pandemic periods, overlooking the emission recovery process after PHEs. Our study is the first to use causal analysis, specifically the Syn-Did method, to bridge these gaps. The Syn-Did outperformed current straightforward comparison by (1) simulating counterfactual emissions in the studied region if the pandemic had not broken out, leveraging data from unaffected regions, (2) comprehensively covering temporal emission data before, during, and after PHEs. We then proposed four carbon resilience indicators based on ATTs computed by Syn-Did. These indicators followed the concept of urban resilience but were adapted to meet decarbonization requirements. Specifically, regions where emissions significantly declined or exceeded previous levels were considered low resilient. Additionally, counterfactual emission trends were taken as pre-pandemic levels rather than assuming unchanged levels in conventional resilience computation⁴⁷. Compared to previous studies, our evaluation provides a deeper understanding of how PHEs affected regional emissions.

Benefiting from the novel research subjects and methods, this study yielded several important findings:

1. CO₂ emissions varied dramatically and were highly uncertain compared to baselines without PHEs. In the power generation sector, the most significant throughout emission decline and increase were $-25,090 \text{ t d}^{-1}$ in Hunan and $26,390 \text{ t d}^{-1}$ in Gansu, respectively. In the industry production sector, the emission variances ranged from $-28,320 \text{ t d}^{-1}$ in Zhejiang to $27,640 \text{ t d}^{-1}$ in Shandong. Additionally, the industry production sector was more resilient than the power generation sector. We attributed the vulnerability of the power sector to its close connections to social aspects, such as residential, commercial, and industrial sectors, making emissions more susceptible to fluctuations during PHEs. In contrast, industry production was more isolated and could maintain normal operations under PHEs. Despite the uncertainty, four distinct emission patterns were identified: (1) fluctuating, (2) insensitive-to-impact pattern, (3) diverging-declining, and (4) diverging-surpassing. Existing studies commonly expected emissions to drop and recover to normal level following the spread and subsequent decline of the virus. However, such convergence was only observed in seven PHEs belonging to the fluctuating pattern, most of which were severe ones widely reported, such as Wuhan, Shanghai, Beijing¹, and Hainan. One reason could be the comprehensive and targeted recovery measures adopted by governments at the end of the pandemic upon recognizing the severity. Most emission variances fluctuated, declined below, or surpassed the baseline levels.
2. Current studies commonly indicate significant emission drops during PHEs due to restrictions in industrial production, transportation, power supply, and residential activities^{10,12–14}. However, our evaluation suggested that the impacts of PHEs were not as substantial as widely perceived during the pandemic. In both sectors, emissions in 40%–50% regional emissions fell into the Type-2 pattern and remained near the counterfactual baselines before PHEs ended. In addition, the regions became more vulnerable when control measures were relaxed after PHEs. The most severe emission divergences occurred when the pandemic ended, namely, Zhejiang ($-60,630 \text{ t d}^{-1}$) and Shandong ($51,280 \text{ t d}^{-1}$) in the power and industry sector, respectively. The average in-resilience in the power and industry sector was 0.76 and 0.78, respectively, considerably exceeding the post-resilience, which were 0.53 and 0.60. The number of regions exhibiting strong in-resilience was also six to eight times greater than those with strong post-resilience. These phenomena imply the potential long-lasting and lagged effect of PHEs.
3. Based on preliminary factor analysis, we identified that PHE-related factors (i.e., colder seasons, longer pandemic or lockdown duration, and a larger number of infection cases) negatively affected regional carbon resilience. This finding complies with our expectation that the severity of PHEs correlates with emission disturbances. In addition, we found that regions with higher energy consumption levels and industry vitality were more resilient, likely due to stronger energy infrastructure and a more isolated and well-managed production environment in these regions. Finally, previous studies pointed out that the consequences of PHEs were more severe in large and developed regions^{10,12–14}, which was partially supported by our findings. First-tier cities, such as Beijing, Shanghai, Shenzhen, and Guangzhou, were clustered in the middle to lower third level in terms of throughout-resilience, in-resilience, and redundancy, and performed relatively well in post-resilience. Some emerging top-tier regions demonstrated strong resilience, such as Hangzhou, Xian, and Qingdao in the power sector and Suzhou, Hangzhou, and Haerbin in the industry sector. In contrast, less developed regions, such as Qinghai, Guiyang, and Gansu, consistently underperformed across most indicators in both sectors.

Based on the previous findings, we propose the following actionable recommendations for policymaking to ensure regional emissions remain predictable and decarbonization resources are allocated more effectively.

1. *Emphasizing data monitoring, sharing, and evaluation.* Our findings demonstrated significant emission variances under PHEs compared to normal levels. Governments should avoid assuming that emissions in affected regions will naturally recover or decline without intervention. Instead, more carbon monitoring and estimating technologies are required. To enable accurate evaluation proposed in the study, it is suggested to collect data from both the affected and unaffected regions during the same periods. This data should include direct references for calculating carbon emissions, such as emission factors and energy consumption data (e.g., fuel and gas usage)⁴⁸. Moreover, to enable Syn-Did simulation, the data need to be fine-grained ideally on a daily basis. These monitoring and estimating tasks necessitate data sharing between government agencies that own and manage data, large companies that provide reliable technologies and data access, and research institutions that undertake data processing and estimation.
2. *Implementing targeted actions based on regional emission patterns.* Decarbonization policymaking during emergencies should differentiate regions based on evaluation results. Specifically, regions with Type-3 emission patterns are likely to experience long-term emission downturn due to adjustments in socio-economic structure, such as the transformation or outflow of power generation and industry companies. More decarbonization resources, especially subsidies for decarbonization strategies, can be temporarily reallocated to regions experiencing Type-4 CO₂ emissions, as these regions are at risk of failing to meet decarbonization goals. Continuous monitoring should be applied to regions encountering Type-1 and Type-2 emissions. For Type-1 emissions, a stable level without significant fluctuation needs to be observed; for Type-2 emissions, post-pandemic variances should be evaluated despite insensitivity to shocks during PHEs. Actions can then be determined based on whether the emission levels are above, below, or close to the normal baseline.
3. *Paying attention to post-pandemic periods.* Policy modifications will be more frequently required when the pandemic ends. Our findings showed that many regions exhibited strong in-resilience, with more than 40% of emission variances being negligible during PHEs. This may be attributed to government's strong mobilization and comprehensive management capabilities to maintain normal power generation and industry production⁴⁹. Additionally, the primary goal during PHEs is emergency handling, such as containing the

- virus, rather than carbon reduction. Furthermore, our findings indicated considerably lower post-resilience across the studied regions. Therefore, subsequent policies, such as carbon taxing and pricing, are needed to prevent unexpected surges in emissions due to compensatory consumption³⁹.
4. *Formulating predictive measures based on regional and PHE characteristics.* Compared to other emergencies such as typhoons and earthquakes, PHEs typically last longer, ranging from several weeks to several months. Since comprehensive Syn-Did evaluation requires post-pandemic data, governments should formulate policies based on regional and PHE factors before PHEs end. For instance, underdeveloped regions often have more factors negatively correlated with carbon resilience, such as low energy consumption, fewer large industrial companies, and poor economic performance. These regions are more susceptible to significant fluctuations in CO₂ emissions, and PHEs with longer duration and severe consequences will worsen the situation. Therefore, once local governments implement PHE control measure, decarbonization policy contingencies should be prepared in advance to address potential emission uncertainty.

This study faces two limitations. First, despite that we identified factors to interpret impacts of PHEs, the analysis was preliminary due to a lack of monthly or daily data of several regional features, hindering more sophisticated analysis, such as collinearity analysis, to minimize bias caused by interdependencies among factors. Additionally, it was not easy to quantify certain factors such as the stringency of prevention measures. Thus, it is again suggested to enrich the data regional features and propose methods for quantifying qualitative factors of PHEs, thereby enabling effective regression and collinearity analysis. Second, we limited the scope to the power and industry sector owing to a lack of high-quality carbon emission data or data enabling accurate emission estimation. Thus, as mentioned in the first policy recommendation, future studies could collect richer data with higher granularity from more sources. For instance, if daily fuel data can be accessed from the energy agency, we can transfer the resilience evaluation process to the transportation sector by replacing the power or industry emissions with emissions estimated based on fuel usage and relevant carbon factors. Similarly, evaluating carbon resilience is also applicable in other sectors contributing to CO₂ emissions, like aviation, agriculture, and residential areas. A comprehensive investigation considering mutual relationships across sectors could reveal more valuable insights for macro policymaking.

Conclusions

This study examined carbon emissions patterns and resilience across various regions during the three-year COVID-19 pandemic in China, focusing on the power generation and industrial production sectors. Causal effects of PHE on carbon emissions were investigated using the Syn-Did method; four carbon resilience indicators were proposed by referring to the urban resilience concept, namely, throughout-resilience, in-resilience, post-resilience, redundancy. Based on the causal analysis and carbon resilience evaluation, four distinct emissions patterns were identified, namely, fluctuating, insensitive-to-impact, diverging-declining, and diverging-surpassing. According to the evaluation results, emissions in 40%–50% of regions demonstrated insensitivity to shocks during PHEs, but widespread poor resilience was observed after the PHEs ended. We identified bottom (e.g., Qinghai, Guiyang) and top (e.g., Jiangsu, Hangzhou) performers in different dimensions of carbon resilience. The factors significantly affecting resilience performance were also identified, such as pandemic severity, regional energy and industry vitality, and socio-economic features. Finally, we proposed policymaking recommendations to address emission uncertainty under PHEs, such as implementing fine-grained data monitoring and sharing, implementing targeted measures based on emission patterns, paying attention to post-pandemic periods, and formulating predictive measure based on regional factors. These findings serves as valuable references for realizing predictable decarbonization strategies, which are also informative in other socio-economic dimensions, e.g., economies and social well-being, when handling shocks causing sustained restrictions of social activities.

Data availability

The data and codes of the paper have been deposited in the Github link: <https://github.com/ErickThoughts/Carbon-resilience>.

Received: 9 May 2024; Accepted: 8 August 2024

Published online: 04 September 2024

References

1. Chen, L. *et al.* Strategies to achieve a carbon neutral society: A review. *Environ. Chem. Lett.* **20**, 2277–2310 (2022).
2. Farghali, M. *et al.* Social, environmental, and economic consequences of integrating renewable energies in the electricity sector: A review. *Environ. Chem. Lett.* **21**, 1381–1418 (2023).
3. Osman, A. I. *et al.* Cost, environmental impact, and resilience of renewable energy under a changing climate: A review. *Environ. Chem. Lett.* **21**, 741–764 (2023).
4. Rockström, J. *et al.* A roadmap for rapid decarbonization. *Science* **355**, 1269–1271 (2017).
5. Loftus, P. J., Cohen, A. M., Long, J. C. & Jenkins, J. D. A critical review of global decarbonization scenarios: What do they tell us about feasibility?. *Wiley Interdiscip. Rev. Clim. Change* **6**, 93–112 (2015).
6. Yuan, H. *et al.* Progress towards the Sustainable Development Goals has been slowed by indirect effects of the COVID-19 pandemic. *Commun. Earth Environ.* **4**, 184 (2023).
7. Li, K. *et al.* The regional impact of the COVID-19 lockdown on the air quality in Ji'nan, China. *Sci. Rep.* **12**, 12099 (2022).
8. Regules, R. *et al.* Climate-related experiences and harms in the wake of the COVID-19 pandemic: Results from a survey of 152,088 Mexican youth. *Sci. Rep.* **13**, 16549 (2023).
9. Kupferschmidt, K. & Wadman, M. End of COVID-19 emergencies sparks debate. *Science* **380**, 566–567 (2023).
10. He, G., Pan, Y. & Tanaka, T. The short-term impacts of COVID-19 lockdown on urban air pollution in China. *Nat. Sustain.* **3**, 1005–1011 (2020).

11. Le Quéré, C. *et al.* Temporary reduction in daily global CO₂ emissions during the COVID-19 forced confinement. *Nat. Clim. Change* **10**, 647–653 (2020).
12. Le Quéré, C. *et al.* Fossil CO₂ emissions in the post-COVID-19 era. *Nat. Clim. Change* **11**, 197–199 (2021).
13. Forster, P. M. *et al.* Current and future global climate impacts resulting from COVID-19. *Nature Climate Change* **10**, 913–919 (2020).
14. Wei, L. *et al.* Black carbon-climate interactions regulate dust burdens over India revealed during COVID-19. *Nat. Commun.* **13**, 1839 (2022).
15. Manyena, B., O'Brien, G., O'Keefe, P. & Rose, J. Disaster resilience: A bounce back or bounce forward ability?. *Local Environ. Int. J. Justice Sustain* **16**, 417–424 (2011).
16. Bogardi, J. J. & Fekete, A. Disaster-related resilience as ability and process: A concept guiding the analysis of response behavior before, during and after extreme events. *Am. J. Clim. Change* **7**, 54–78 (2018).
17. Huang, G., Li, D., Zhu, X. & Zhu, J. Influencing factors and their influencing mechanisms on urban resilience in China. *Sustain. Cities Soc.* **74**, 103210 (2021).
18. Holling, C. S. Resilience and stability of ecological systems. (1973).
19. Sutton, J. & Arku, G. Regional economic resilience: Towards a system approach. *Reg. Stud. Reg. Sci.* **9**, 497–512 (2022).
20. Meerow, S., Newell, J. P. & Stults, M. Defining urban resilience: A review. *Landscape Urban Plan.* **147**, 38–49 (2016).
21. Ribeiro, P. J. G. & Gonçalves, L. A. P. J. Urban resilience: A conceptual framework. *Sustain. Cities Soc.* **50**, 101625 (2019).
22. Lee, S., Kim, J. & Cho, K. Temporal dynamics of public transportation ridership in Seoul before, during, and after COVID-19 from urban resilience perspective. *Sci. Rep.* **14**, 8981 (2024).
23. Pendall, R., Foster, K. A. & Cowell, M. Resilience and regions: Building understanding of the metaphor. *Cambridge J. Regions Econ. Soc.* **3**, 71–84 (2010).
24. Arkhangelsky, D., Athey, S., Hirshberg, D. A., Imbens, G. W. & Wager, S. *Synthetic Difference in Differences* (National Bureau of Economic Research, 2019).
25. Lopez Bernal, J., Cummins, S. & Gasparrini, A. Difference in difference, controlled interrupted time series and synthetic controls. *Int. J. Epidemiol.* **48**, 2062–2063 (2019).
26. Liu, Z. *et al.* Challenges and opportunities for carbon neutrality in China. *Nat. Rev. Earth Environ.* **3**, 141–155 (2022).
27. Liu, W., Yue, X.-G. & Tchounwou, P. B. Vol. 17, 2304 (MDPI, 2020).
28. Shan, Y. *et al.* Impacts of COVID-19 and fiscal stimuli on global emissions and the Paris Agreement. *Nat. Clim. Change* **11**, 200–206 (2021).
29. Shen, L. *et al.* Improved coupling analysis on the coordination between socio-economy and carbon emission. *Ecol. Indic.* **94**, 357–366 (2018).
30. Bruninx, K. & Ovaere, M. COVID-19, Green Deal and recovery plan permanently change emissions and prices in EU ETS Phase IV. *Nat. Commun.* **13**, 1165 (2022).
31. Yi, W., Yuan, X., Lu, Q., Lin, P. & Wang, Q. The Development Report of China Metropolitan Area in 2018. (2018).
32. Qi, J. *et al.* Short-and medium-term impacts of strict anti-contagion policies on non-COVID-19 mortality in China. *Nat. Hum. Behav.* **6**, 55–63 (2022).
33. Liu, Z. *et al.* Near-real-time monitoring of global CO₂ emissions reveals the effects of the COVID-19 pandemic. *Nat. Commun.* **11**, 5172 (2020).
34. Liu, Z. *et al.* Global patterns of daily CO₂ emissions reductions in the first year of COVID-19. *Nat. Geosci.* **15**, 615–620 (2022).
35. Arkhangelsky, D., Athey, S., Hirshberg, D. A., Imbens, G. W. & Wager, S. Synthetic difference-in-differences. *Am. Econ. Rev.* **111**, 4088–4118 (2021).
36. Rebekić, A., Lončarić, Z., Petrović, S. & Marić, S. Pearson's or Spearman's correlation coefficient-which one to use?. *Poljoprivreda* **21**, 47–54 (2015).
37. Rana, R. & Singhal, R. Chi-square test and its application in hypothesis testing. *J. Pract. Cardiovasc. Sci.* **1**, 69 (2015).
38. Yang, Z. *et al.* Clinical characteristics, transmissibility, pathogenicity, susceptible populations, and re-infectivity of prominent COVID-19 variants. *Aging Dis.* **13**, 402 (2022).
39. Davis, S. J. *et al.* Emissions rebound from the COVID-19 pandemic. *Nat. Clim. Change* **12**, 412–414 (2022).
40. Luke, M., Somani, P., Cotterman, T., Suri, D. & Lee, S. J. No COVID-19 climate silver lining in the US power sector. *Nat. Commun.* **12**, 4675 (2021).
41. Habibi, Z., Habibi, H. & Mohammadi, M. A. The potential impact of COVID-19 on the Chinese GDP, trade, and economy. *Economics* **10**, 73 (2022).
42. Hans, F., Woollands, S., Nascimento, L., Höhne, N. & Kuramochi, T. Unpacking the COVID-19 rescue and recovery spending: an assessment of implications on greenhouse gas emissions towards 2030 for key emitters. *Clim. Action* **1**, 3 (2022).
43. Nottmeyer, L. *et al.* The association of COVID-19 incidence with temperature, humidity, and UV radiation—A global multi-city analysis. *Sci. Total Environ.* **854**, 158636 (2023).
44. Song, Z. & Kuenzer, C. Coal fires in China over the last decade: A comprehensive review. *Int. J. Coal Geol.* **133**, 72–99 (2014).
45. Tang, B. *et al.* Lessons drawn from China and South Korea for managing COVID-19 epidemic: Insights from a comparative modeling study. *ISA Trans.* **124**, 164–175 (2022).
46. Li, L., Zhang, S., Wang, J., Yang, X. & Wang, L. Governing public health emergencies during the coronavirus disease outbreak: Lessons from four Chinese cities in the first wave. *Urban Stud.* **60**, 1750–1770 (2023).
47. Sutton, J., Arku, G., Sadler, R., Hutchenreuther, J. & Buzzelli, M. Practitioners' ability to retool the economy: The role of agency in local economic resilience to plant closures in Ontario. *Growth Change* **55**, e12716 (2024).
48. Liu, J. *et al.* Multi-scale urban passenger transportation CO₂ emission calculation platform for smart mobility management. *Appl. Energy* **331**, 120407 (2023).
49. He, A. J., Shi, Y. & Liu, H. Crisis governance, Chinese style: Distinctive features of China's response to the Covid-19 pandemic. *Policy Design Pract.* **3**, 242–258 (2020).

Acknowledgements

This study was supported by grants from the National Natural Science Foundation of China (52208324, 72204248), Guangdong Basic and Applied Basic Research Foundation (2023A1515011162), Shenzhen Science and Technology Program (RCBS20221008093307015), Research Grants Council of the Hong Kong SAR of China (No.15219422, G-HKU502/22).

Author contributions

Chengke Wu and Xiao Li: conducted the data analysis and wrote the main manuscript texts Zisheng Liu, Juan Wang, and Fangyun Xie: collected all data and completed data pre-processing Rui Jiang: assisted in data analysis, revised the manuscript and completed figure visualization Yue Teng: revised all tables and figures, and

organized the expert survey Zhile Yang: funding and resource, supervision, project management, and assisted in data collection.

Competing interests

The authors declare no competing interests.

Additional information

Supplementary Information The online version contains supplementary material available at <https://doi.org/10.1038/s41598-024-69785-7>.

Correspondence and requests for materials should be addressed to Z.Y.

Reprints and permissions information is available at www.nature.com/reprints.

Publisher's note Springer Nature remains neutral with regard to jurisdictional claims in published maps and institutional affiliations.

Open Access This article is licensed under a Creative Commons Attribution-NonCommercial-NoDerivatives 4.0 International License, which permits any non-commercial use, sharing, distribution and reproduction in any medium or format, as long as you give appropriate credit to the original author(s) and the source, provide a link to the Creative Commons licence, and indicate if you modified the licensed material. You do not have permission under this licence to share adapted material derived from this article or parts of it. The images or other third party material in this article are included in the article's Creative Commons licence, unless indicated otherwise in a credit line to the material. If material is not included in the article's Creative Commons licence and your intended use is not permitted by statutory regulation or exceeds the permitted use, you will need to obtain permission directly from the copyright holder. To view a copy of this licence, visit <http://creativecommons.org/licenses/by-nc-nd/4.0/>.

© The Author(s) 2024